



*Conference Proceedings of the 5th Asia Pacific Luminescence and Electron Spin Resonance Dating Conference
October 15th-17th, 2018, Beijing, China*

Guest Editor: Grzegorz Adamiec

CHRONOLOGY OF THE HUXUSHAN PALEOLITHIC SITE IN SOUTH CHINA: INFERRED FROM MULTIPLE LUMINESCENCE DATING TECHNIQUES

HAI-CHENG LAI¹, YI-YUAN LI², JIA-FU ZHANG¹ and LIPING ZHOU¹

¹*Key Laboratory for Earth Surface Processes, Department of Geography, College of Urban and Environmental Sciences, Peking University, Beijing 100871, China*

²*Institute of Cultural Relics and Archaeology of Hunan Province, Changsha 410008, China*

Received 16 February 2019

Accepted 9 February 2021

Abstract: The Huxushan archaeological site in northern Hunan Province, China, was recently excavated, from which stone tools including handaxes were unearthed. The deposits of the site are chemically weathered, which makes it difficult to date the site using numerical dating techniques except for optically stimulated luminescence (OSL) method. Here, we used various luminescence procedures including single-aliquot regenerative-dose (SAR), sensitivity-corrected multiple-aliquot regenerative-dose (SMAR) and thermally transferred optically stimulated luminescence (TT-OSL) SAR procedures on fine-grained quartz, and two-step post-infrared infrared stimulated luminescence (pIRIR) and multi-elevated-temperature pIRIR (MET-pIRIR) procedures on fine polymineral fractions. The results show that the fine quartz grains have excellent luminescence properties and the quartz SAR-, SMAR- and TT-OSL ages for the samples agree with each other and in stratigraphical order except for one sample. The fine polymineral fractions exhibited relatively weak pIRIR and MET-pIRIR signals, resulting in difficulty in constructing the dose-response curve for MET-pIRIR signals and the stratigraphically inconsistent pIRIR_(100, 275) ages. The seven samples yielded their quartz OSL ages ranging from about 62 ka to 133 ka. The two samples from the cultural layer was dated to 78 to 92 ka using different procedures on fine quartz. However, given the systematically older pIRIR ages obtained with the fine polymineral grains for the two samples, their quartz OSL ages are considered to represent the minimal ages of this layer, and their pIRIR_(100, 275) ages of 118 and 110 ka represent the upper age limit, indicating that the site was occupied by hominins during Marine Isotope Stage 5.

Keywords: fine quartz, fine polymineral fractions, various luminescence protocols, weak pIRIR signals, stratigraphically consistent quartz OSL ages, Paleolithic site.

1. INTRODUCTION

In recent years, substantial progress has been achieved in the discoveries and studies of the Chinese Paleolithic, especially for the Late Pleistocene period (Lu *et al.*, 2011; Sun *et al.*, 2012; Gao, 2013; Liu *et al.*, 2015; Zhang *et al.*, 2018). The fact that numerous open-air Paleolithic sites have recently been found and excavated in south China implies that south China plays a pivotal role in understanding the origin and prehistory of humanity in East Asia (Liu *et al.*, 2008; Zhu *et al.*, 2008). In addition, according to genetic studies (Chu *et al.*, 1998; Piazza 1998; Wang and Li, 2013), south China is also the possible gateway for hominin to migrate into the hinterland of China, and thereby more detailed analyses of Paleolithic sites in south China are of great archaeological significance. However, it is hard to construct their chronological framework, because an intensive chemical weathering of the deposits results in the lack of suitable materials for numerical dating such as radiocarbon dating.

Optically stimulated luminescence (OSL) dating provides an estimate of the time elapsed since luminescent minerals, such as ubiquitous quartz or feldspar, were last exposed to sunlight (Huntley *et al.*, 1985; Aitken and Smith, 1988), and it directly determines the burial ages of sediments. This method has already been extensively applied to Paleolithic archeology (Slimak *et al.*, 2011; Roberts *et al.*, 2015; Li *et al.*, 2017; Hu *et al.*, 2019). Various procedures have been developed to measure equivalent dose (D_e) of dated materials, including single-aliquot regenerative-dose (SAR) (Murray and Wintle, 2000), sensitivity-corrected multiple-aliquot regenerative dose (SMAR) (Zhou and Shackleton, 2001; Lu *et al.*, 2007) and thermally-transfer SAR (TT-OSL SAR) (Wang *et al.*, 2006) procedures on quartz, and post-infrared infrared stimulated luminescence (pIRIR) (two-step pIRIR and multi-elevated-temperature pIRIR (MET-pIRIR)) procedures on potassium feldspars (Thomsen *et al.*, 2008; Thiel *et al.*, 2011; Li and Li, 2011, 2012a, 2012b).

In this paper, we used the above procedures on the fine-grained quartz and polymineral fractions of seven samples from the Huxushan Paleolithic site in northern Hunan Province, China. The luminescence ages obtained using the procedures were compared to evaluate their reliability, and the chronology of the site was established.

2. GEOMORPHOLOGY, STRATIGRAPHY AND ARCHAEOLOGY

The Paleolithic site of Huxushan ($28^{\circ}56'20''\text{N}$, $112^{\circ}17'22''\text{E}$) is located at the Chishan Island surrounded by the Dongting Lake in the northern part of Hunan Province, China (Fig. 1a). The Dongting Lake, located in the middle reach of the Yangtze River, is the second largest freshwater lake in China. The Lishui, Yuanjiang and Zishui rivers in the study area discharge water into the lake from the northwest, west and south, respectively. The length and width of the island are about 30 and 4 km, respectively. The elevation of the island is between 30 m above sea level (asl) in the north, and 80 m asl in the south. The covering sediments are characterized by the great thickness of red earth. The region is located in the humid subtropical monsoon climate zone, and has an annual mean precipitation of 1322 mm and the mean monthly temperature ranging from 4.3°C (January) to 29.1°C (July).

The Huxushan site is situated on the western gentle slope of a hill, and is one of the discoveries in this region during the archeological survey in 2016 led by archeologist Yi-Yuan Li from the Institute of Cultural Relics and Archeology of Hunan Province. The area of 350 m^2 of the site has been excavated, and the deposits are divided into five layers numbered 1 to 5, from top to bottom (Fig. 1b). Layer 1 (0.2–0.8 m thick) is topsoil consisting of grey-yellow silty clay disturbed by human activities. Layer 2 (0.8–1.0 m thick) is composed of reddish-brown silty clay. Layers 3–5 comprise mottled red clay with worm- or net-like white stripes. Layer 3 (0.5–1.2 m thick) is

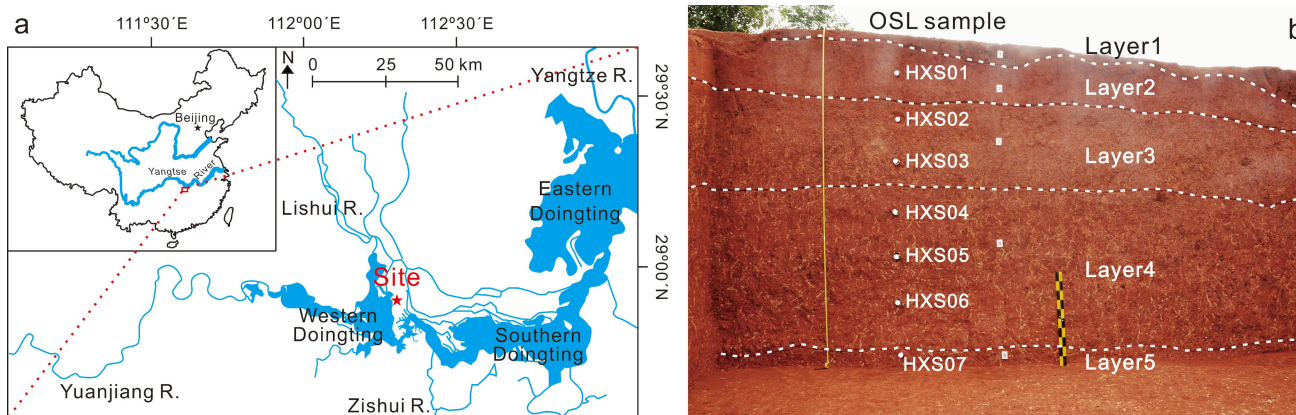


Fig. 1. (a) Map showing the location of the study site, and (b) photograph of the excavation pit showing the stratigraphy and the positions of OSL samples.

reticulate red silty clay that is characterized by light yellow veins and massive Fe-Mn nodules. Layer 4 (2.0–2.5 m thick) consists of dark reddish-brown reticulate silty clay with a few Fe-Mn nodules. Layer 5 (0.4–0.5 m thick) is composed of deep reddish reticulate silty clay with short and thick white veins.

Stone artifacts were unearthed largely from Layer 3 and a few from the lower part of Layer 2 and the upper part of Layer 4. Raw materials in excavated assemblages are mainly comprised of quartz sandstone, quartz, siliceous limestone, quartzite and relatively small quantities of chert. We deduce that the raw materials were from the adjacent rivers because of the consistency in lithological characteristics and sedimentary types between the raw materials and the gravels found in the modern rivers. The stone artifacts include cobbles (manuports), cores, flakes and tools, suggesting a suit of incomplete technological assemblage. The sizes of lithic assemblage primarily have large tools and a few small productions such as flakes and scrapers. The cores are mainly composed of ordinary cores including single, dual or multiplatform and the others are discoidal and multi-faced. The flakes reflect low efficiency in using raw materials. The stone tools include chopping tools, picks, hand axes and heavy scrapers. Of these tools, though heavy tools are dominated, the number of picks and hand axes are relatively few but they are typical. The picks are triangular and tongue-shaped. The hand axes are made of siliceous breccia with delicately bifacial retouching.

3. METHODS

Sampling and sample preparation

Seven sediment samples were collected from the stratigraphic profile of the south wall of the excavation pit for luminescence dating at the Luminescence Dating Laboratory of Peking University. The samples were taken by hammering stainless steel tubes (5 cm in diameter and 20 cm in length) horizontally into the vertical wall of freshly cleaned exposures. The tubes were then covered with aluminum foil and sealed with opaque tape.

Sample preparation for D_e determination was done under subdued red light in the dark room using the procedure described in Zhang and Zhou (2007). Carbonates in the samples were dissolved in 10% HCl acid, and organic matter was oxidized in 30% H_2O_2 . The samples were then separated by wet sieving to attempt to obtain medium-grained (45–63 μm) fractions, but failed to obtain enough amount of the grains for D_e measurements. The polymineral fine (4–11 μm) grains were obtained by settling after Stokes' Law. To obtain fine-grained quartz, some of the polymineral fine-grained fractions obtained were further purified with silica saturated fluorosilicic acid (H_2SiF_6) for three days followed by treatment with 10% HCl to remove any fluorides produced. The purity of the quartz extracts was checked by infrared stimulation followed by an OSL measurement. The IRSL signals detect-

ed were less than 0.1% of the OSL signal for all seven samples, indicating that feldspar contaminants were completely removed. The fine quartz and polymineral grains were respectively dispersed in acetone and then deposited onto 0.97 cm diameter aluminum discs for D_e measurements.

Equivalent dose determination

All luminescence measurements were performed in an automated Risø TL/OSL-20 luminescence reader. Irradiations were carried out using a $^{90}\text{Sr}/^{90}\text{Y}$ beta source equipped in the reader. Quartz grains were stimulated using blue LEDs ($\lambda = 470 \pm 30$ nm), and the OSL signal was detected using an EMI 9235QA photomultiplier tube (PMT) with a 7.5 mm Hoya U-340 filter in front. Polymineral grains were stimulated using IR diodes ($\lambda = 870 \pm 40$ nm) with the IRSL signal collected through the same PMT with a Schott BG39/Corning 7-59 filter combination in front (Bøtter-Jensen *et al.*, 2003).

Three procedures in **Table 1** were employed to determine the equivalent dose of quartz extracts. In the SAR protocol (Murray and Wintle, 2000, 2003), regenerative beta doses include a zero-dose used for monitoring recuperation effects and a repeat of the first regeneration dose used for checking the reproducibility of the sensitivity correction (i.e. recycling ratio). Test doses were irradiated immediately after measuring natural or regenerative-dose OSL signals (L_i) to produce the OSL signal (T_i) for correcting sensitivity changes due to preheating/OSL measurements. D_e value is obtained by projecting the corrected natural OSL intensity (L_N/T_N) onto the dose-response curve (DRC) constructed using the corrected regenerative-dose OSL intensity (L_i/T_i). Preheat of 250°C for 10 s (determined from preheat plateau tests, see the following section) and a cut-heat of 160°C were applied. A 280°C blue LED stimulations for 40 s was conducted at the end of each round of the measurement to reduce recuperation. The SMAR protocol (Zhou and Shackleton, 2001; Lu *et al.*, 2007) was also used for the quartz extracts under the same conditions as in the SAR protocol. Six regeneration doses were performed, and their corrected OSL signals were used to construct DRC. Three aliquots were used for each regeneration dose.

In order to check the upper age limit of the quartz OSL-SAR and OSL-SMAR methods for our samples, the samples were also measured using the TT-OSL procedure proposed by Wang *et al.* (2006) (**Table 1**). The TT-OSL can be separated into two parts, the recuperated OSL (Re-OSL) and basic transferred OSL (BT-OSL). It is shown that the Re-OSL signal continues to grow with increasing dose up to 20, 000 Gy, while this is not the case for the BT-OSL signal. Using the equation $L_{\text{Re-OSL}} = [L_{\text{TT-OSL}}/T_{\text{TT-OSL}}] - [L_{\text{BT-OSL}}/T_{\text{BT-OSL}}]$, Wang *et al.* (2006) showed that the ages for loess using both the OSL signal and the Re-OSL signal were consistent from modern to ~130 ka, demonstrating that Re-OSL could be used for dating. Here six aliquots were measured to obtain the

Table 1. Protocols used for D_e measurements of fine quartz grains.

Step OSL-SAR protocol	Observed	Step OSL-SMAR protocol	Observed	Step TT-OSL SAR procedure	Observed
1 Give dose, D_i		Part 1 Detection of natural OSL signal		Part 1 Detection of thermal-transferred OSL signal	
2 Preheating at 250°C for 10 s		1-1 Preheating at 250°C for 10 s		1-1 Give dose, D_i	
3 Blue stimulation at 125°C for 40 s	L_i	1-2 Blue stimulation at 125°C for 40 s	L_n	1-2 Preheating at 250°C for 10 s	
4 Give test dose, D_t (18.3 Gy)		1-3 Give test dose, D_t (18.3 Gy)		1-3 Blue stimulation at 125°C for 300 s	
5 Cut heat at 160°C for 5 s		1-4 Cut heat at 160°C for 5 s		1-4 Preheating at 250°C for 10 s	
6 Blue stimulation at 125°C for 40 s	T_i	1-5 Blue stimulation at 125°C for 40 s	T_n	1-5 Blue stimulation at 125°C for 40 s	L_{TTOSL}
7 Blue stimulation at 280°C for 40 s		Part 2 Detection of regenerative OSL signal		1-6 Give test dose, D_t (18.3 Gy)	
8 Return to step 1		2-1 Bleaching at 125°C for 60 s		1-7 Cut heat at 160°C for 5 s	
		2-2 Give dose, D_i		1-8 Blue stimulation at 125°C for 100 s	T_{TTOSL}
		2-3 Preheating at 250°C for 10 s		Part 2 Detection of basic-transferred OSL signal	
		2-4 Blue stimulation at 125°C for 40 s	L_i	2-1 Annealing to 300°C for 10 s	
		2-5 Give test dose, D_t (18.3 Gy)		2-2 Blue stimulation at 125°C for 100 s	
		2-6 Cut heat at 160°C for 5 s		2-3 Preheating at 250°C for 10 s	
		2-7 Blue stimulation at 125°C for 40 s	T_i	2-4 Blue stimulation at 125°C for 100 s	L_{BTOSL}
				2-5 Give test dose, D_t (18.3 Gy)	
				2-6 Cut heat at 220°C for 10 s	
				2-7 Blue stimulation at 125°C for 100 s	T_{BTOSL}
				2-8 Blue stimulation at 280°C for 100 s	

Note that $D_i=0$ when measuring natural signals.

intensity of natural TT-OSL (L_{TT-OSL}) and basic transferred OSL (L_{BT-OSL}), respectively. Test doses were used immediately to obtain T_{TT-OSL} and T_{BT-OSL} signals in exactly the same way as in the SAR protocol. The Re-OSL D_e value was then obtained by projecting the corrected natural L_{Re-OSL} intensity to the DRC constructed using the corrected regenerated L_{Re-OSL} intensities. For quartz extracts, the initial 0.64 s signal minus the last 3.2 s integral as a background in the decay curves was used for dose calculation.

Two procedures listed in **Table 2** were used to determine the equivalent doses of the polymineral fine grains. In the MET-pIRIR protocol proposed by Li and Li (2011, 2012a), the preheat of 320°C for 60 s was applied after both regenerative and test dose to clear great influence from residual signals from measurements (steps 7 and 14). The regenerative and test dose IRSL signals after preheat were measured for 100 s at stimulated temperatures of 50, 100, 150, 200, 250, 290°C, respectively. A 100 s IR bleaching at 325°C was applied at the end of each cycle to clear recuperation. The two-step pIRIR protocol was also employed to determine the equivalent doses of the fine-grained polymineral fractions (Thomsen *et al.*, 2008; Thiel *et al.*, 2011; Buylaert *et al.*, 2012), in which the polymineral aliquots were preheated at 320°C for 60 s, and IR stimulation time is 200 s. The first IR stimulation temperature was 100°C (IRSL signal) determined by D_e plateau tests (see the following section for details) (Li and Li, 2012a), and the subsequent IR stimulation temperature was 275°C (post-IR IRSL signal,

pIRIR_(100, 275)). The IR clean-out at the end of each SAR cycle was carried out at 325°C for 200 s. The first 2 s signal minus a background estimated from the last 50 s in the decay curves was used for dose calculation. It is noted that the experiments for anomalous fading and residual doses were not carried out (see the following section for details).

Dose rate measurements

The annual dose estimation was based on U, Th and K concentrations. U and Th concentrations were determined by laser ablation inductively coupled plasma mass spectrometer (ICP-MS), and K concentrations were determined by a Wavelength Dispersive X-Ray Fluorescence spectrometer. Water contents (weight water/dry sediment weight) for all samples were measured in the laboratory, but the experiment results (13–14%) were probably lower than the natural values since the sediment section had been exposed to air for a long time. Therefore, we prefer to use a higher value of 23% obtained by similar samples from the Fengshuzui site (Zhang *et al.*, 2018) close to the studied site. U, Th, K and water contents were assumed to have an uncertainty of 5% to cover analytical errors. The cosmic ray contribution for each sample was calculated as a function of depth, altitude, and geomagnetic latitude (Prescott and Hutton, 1994). The α -efficiency was taken as 0.04 ± 0.02 for quartz and 0.08 ± 0.02 for polymineral grains, respectively (Lai and Brückner, 2008). Finally, annual dose rates and ages were calculated using the DRAC calculator (v1.2) (Durcan *et al.*, 2015).

Table 2. Procedures used for D_e measurements of fine polymineral grains.

Step	MET-pIRIR procedure	Observed	Step	Two-step pIRIR procedure	Observed
1	Give dose, D_i		1	Give dose, D_i	
2	Preheating at 320°C for 60 s		2	Preheating at 320°C for 60 s	
3	Infrared stimulation at 50°C for 100 s	$L_{x(50)}$	3	Infrared stimulation at 100°C for 200 s	
4	Infrared stimulation at 150°C for 100 s	$L_{x(150)}$	4	Infrared stimulation at 275°C for 200 s	L_i
5	Infrared stimulation at 200°C for 100 s	$L_{x(200)}$	5	Give test dose, D_t (91.5 Gy)	
6	Infrared stimulation at 250°C for 100 s	$L_{x(250)}$	6	Cut heat at 320°C for 60 s	
7	Infrared stimulation at 290°C for 100 s	$L_{x(290)}$	7	Infrared stimulation at 100°C for 200 s	
8	Give test dose, D_t (91.5 Gy)		8	Infrared stimulation at 275°C for 200 s	T_i
9	Preheating at 320°C for 60 s		9	Infrared stimulation at 325°C for 200 s	
10	Infrared stimulation at 50°C for 100 s	$T_{x(50)}$	10	Return to step 1	
11	Infrared stimulation at 150°C for 100 s	$T_{x(150)}$			
12	Infrared stimulation at 200°C for 100 s	$T_{x(200)}$			
13	Infrared stimulation at 250°C for 100 s	$T_{x(250)}$			
14	Infrared stimulation at 290°C for 100 s	$T_{x(290)}$			
15	IR bleaching at 325°C for 100 s				
16	Return to step 1				

Note that $D=0$ when measuring natural signals.

4. RESULTS

Luminescence properties and ages of quartz extracts

Examples of quartz OSL decay curves and SAR- and SMAR-OSL DRCs for our studied samples are illustrated in Fig. 2. Note that the DRCs for all samples were fitted with a single exponential saturation (SE) or saturating exponential plus linear function (SEPL) using the Risø luminescence Analyst version 4.53 software. The shine-down curve indicates that the quartz natural OSL signal is reduced to 4.3% of its initial intensity after 0.96 s of blue stimulation at the sample temperature of 125°C, demonstrating that the quartz grains are very bright, and the

OSL signal is dominated by the fast component. The DRCs demonstrate that the OSL signals are not saturated at a dose up to about 1000 Gy, and have the characteristic saturation doses (D_{01} and D_{02}) of 35 and 464 Gy, if the curve is fitted with a double saturating exponential function. The shapes of the SAR- and SMAR-OSL DRCs are identical when regeneration dose is less than about 400 Gy if errors are considered. The recycling ratios for all samples using the SAR protocol are within the range of 1.0 ± 0.1 and the recuperation less than 5%, suggesting that the sensitivity correction for these samples is successful and thermal transfer negligible.

Preheat plateau tests were carried out to determine a suitable preheat temperature for quartz aliquots. The D_e values of aliquots from sample L3478 were measured using the SAR procedure in Table 1 with different preheat temperatures ranging from 180 to 280°C at 20°C increments. Three aliquots were measured at each preheat temperature. The results shown in Fig. 3a indicate that there is no dependency on D_e values on preheat temperature in the range of 200–280°C. The recycling ratios are within the range of 0.9 to 1.1, and the recuperation is less than 2% for all samples (Fig. 3b), indicating that the preheat temperatures of 200–280°C are suitable for D_e determination on the quartz aliquots.

Dose recovery tests were also performed on the same sample as used in the preheat plateau tests to confirm the results of the preheat plateau tests. Prior to irradiating a laboratory dose, the natural OSL signals were removed by two 100 s blue light (blue LED) exposures at room temperature, separated by a 10 ks pause to allow any photo-transferred charge in the 110°C thermoluminescence trap to decay. The bleached aliquots were then irradiated with a given dose approximately equivalent to the D_e values of the sample, and the irradiated aliquots were measured using the SAR procedure in Table 1.

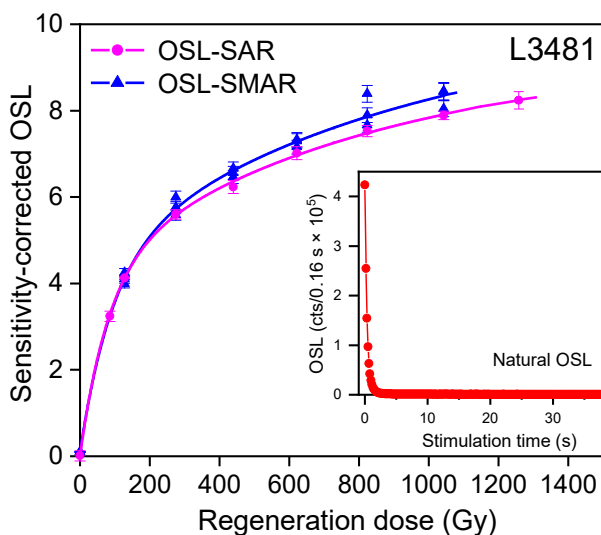


Fig. 2. Comparison of dose-response curves constructed using the quartz OSL-SAR and OSL-SMAR protocols for sample L3481. The inset shows a natural decay curve for the same aliquot.

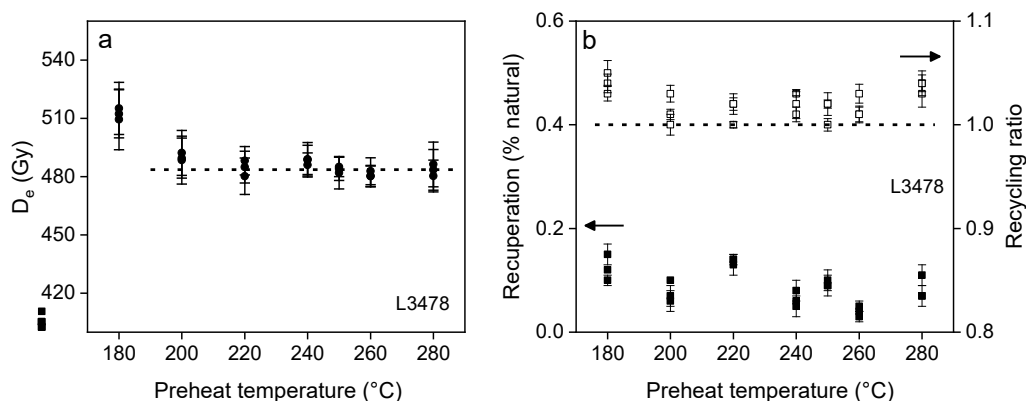


Fig. 3. (a) Plot of D_e values as a function of preheat temperature in the range of 180 and 280°C at 20°C increments for sample L3478, and (b) recycling ratios and recuperation against preheat temperature. Three aliquots were determined at each preheat temperature.

Three aliquots were measured for each preheat temperature, and the results are shown in **Fig. 4**. It shows that the ratios of measured dose to the given dose (dose recovery ratio) are closest to unity at the preheat temperature of 250°C. Therefore, the preheat of 250°C for 10 s was used in the quartz OSL-SAR, OSL-SMAR and TT-OSL SAR procedures.

Examples of the decay curves of the natural TT-OSL (**Fig. 5a**) and BT-OSL (**Fig. 5b**) signals and the regeneration dose TT-OSL (**Fig. 5c**) and BT-OSL (**Fig. 5d**) signals are shown in **Fig. 5**. It is evident that there was a significant rise in the intensities of L_{TT-OSL} with increasing doses, and this is not the case for L_{BT-OSL} . The corrected recuperated intensity, L_{Re-OSL} , was obtained by the equation (mentioned above). The corresponding DRCs and one of the L_{Re-OSL} signals are shown in **Fig. 5e** and **5f**,

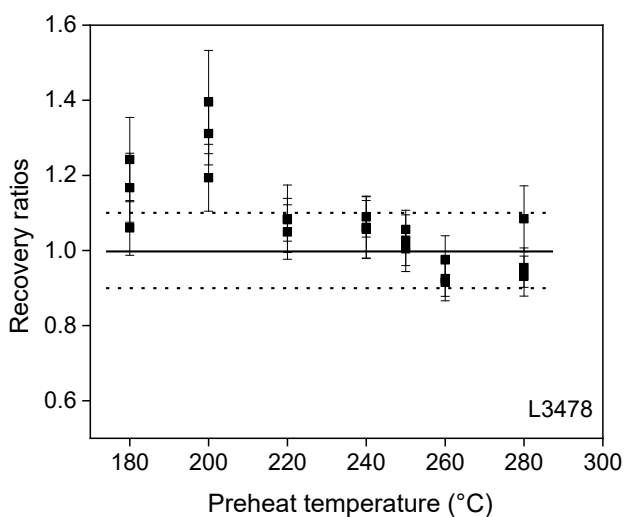


Fig. 4. Plot of recovery ratios versus preheat temperature for sample L3478. Three aliquots were tested at each preheat temperature.

respectively, for which the recycling ratios fall into the acceptance range of 0.9–1.1, and recuperation is 1.01 ± 0.03 . The DRC in **Fig. 5f** was fitted with a single saturating exponential, the D_e value obtained is much less than the D_0 value of about 470 Gy for the curve. In order to determine the residual TT-OSL signal of the studied samples, the natural aliquots of sample L3481 were exposed to light from a solar simulator (SOL2, Hönle UVACUBE400) for 1 min, 9 h and 2 days, respectively, and then measured using the TT-OSL procedure in **Table 1**. Three aliquots were used for each bleaching time. The residual TT-OSL D_e values of 230.5 ± 10.1 Gy, 70.0 ± 5.7 Gy and 33.4 ± 1.6 Gy were obtained for the three bleaching times, respectively. The dose of 33.4 Gy was taken as a residual TT-OSL dose for subtraction for all samples.

The dose rates and D_e values obtained using the above three procedures on fine-grained quartz are summarized and listed in **Table 3**. It shows that the calculated dose rates range from 4.3 to 3.5 Gy/ka, and the D_e values varying from about 269 to 460 Gy obtained using the three procedures. The ages were obtained by dividing the D_e values by the dose rates and listed in **Table 3** and displayed in **Fig. 6**. The top sample (sample L3475) was dated to SAR-OSL 67 ± 4 ka, SMAR-OSL 66 ± 4 ka and TT-OSL 62 ± 4 ka, and the bottom sample (sample L3481) to SAR-OSL 133 ± 9 ka, SMAR-OSL 123 ± 9 ka and TT-OSL 127 ± 9 ka. The figure demonstrates that the SAR-OSL, SMAR-OSL and TT-OSL ages for each sample are consistent within errors except for sample L3478, and they are in stratigraphical order.

PIRIR ages of polymineral grains

All the samples show relatively dim IRSL, pIRIR and MET-pIRIR signals, and their natural intensities decrease as depth increases (**Figs. 7–9**). Note that the intensity of the natural IRSL signals measured at the sample temperature of 250°C are much larger than at lower temperatures

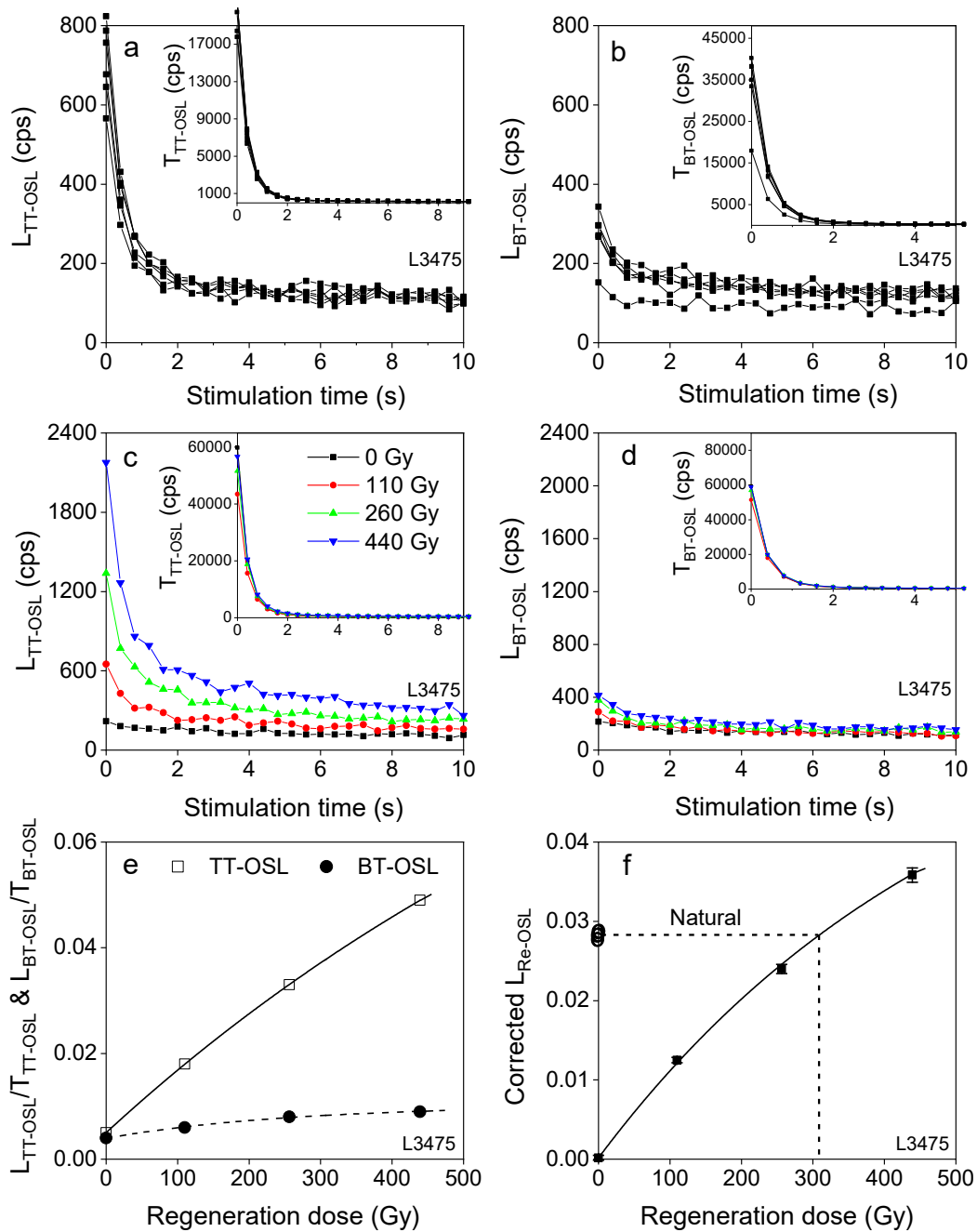


Fig. 5. Decay curves of natural (a) thermally-transferred (TT) and (b) basic-transferred (BT) OSL, regenerative-dose (c) TT-OSL and (d) BT-OSL signals; dose-response curves for the sensitivity-corrected TT-OSL (square) and BT-OSL (solid circle) signals (e) and recuperated OSL (Re-OSL) signals (f). The insets in (a–d) showing the test-dose (18.3 Gy) OSL signals following natural and regenerative-dose OSL measurements.

(Fig. 7). Fig. 7 demonstrates that the MET-pIRIR signals are very dim and close to the noise background, and this is especially the case for the test dose (91.5 Gy) signals. The dim MET-pIRIR signals result in very large uncertainties in MET-pIRIR D_e values. In this case, the MET-pIRIR D_e s of the samples were not further determined.

In the two-step pIRIR procedure (Table 2), the effect of the first IR stimulation temperature on pIRIR D_e val-

ues was tested using the temperatures of 50, 100, 150 and 200°C, respectively, and the results shown in Fig. 10 indicate that the pIRIR D_e values are independent of the first stimulation temperatures between 50 and 150°C, and the recycling ratios are close to unity and the recuperations less than 5%. Therefore, here the sample temperature of 100°C was used for the IRSL signal measurements before measuring the pIRIR signals at 275°C. Two

Table 3. The results of luminescence dating of fine-grained quartz using different procedures and fine polymineral grains using the pIRIR_(100, 275) procedure.

Lab No.	Layer	Depth (cm)	U (ppm)	Th (ppm)	K (%)	Water (%)	Cosmic dose rate (Gy/ka) ^a	Mineral	Number of Aliquot ^b	Method	Dose rate (Gy ka ⁻¹)	D _e (Gy)	Age (ka)
L3475	2	50	4.1	19.7	1.8	23.0	0.20	Quartz	9	OSL-SAR	4.3 ± 0.3	290.8 ± 7.3	67 ± 4
									3(6)	OSL-SMAR		283.1 ± 5.1	66 ± 4
									6(6)	TT-OSL SAR		268.9 ± 8.9	62 ± 4
									3	pIRIR_(100, 275)	5.1 ± 0.3	389.5 ± 27.8	77 ± 7
L3476	3	100	3.7	18.0	1.7	23.0	0.18	Quartz	9	OSL-SAR	4.0 ± 0.2	361.8 ± 9.6	91 ± 6
									3(6)	OSL-SMAR		334.7 ± 10.1	84 ± 6
									6(6)	TT-OSL SAR		307.5 ± 21.7	78 ± 7
									3	pIRIR_(100, 275)	4.6 ± 0.3	546.3 ± 24.4	118 ± 8
L3477	3	150	3.7	19.0	1.7	23.0	0.17	Quartz	9	OSL-SAR	4.0 ± 0.2	371.4 ± 21.0	92 ± 8
									3(6)	OSL-SMAR		364.4 ± 25.7	90 ± 8
									6(6)	TT-OSL SAR		334.0 ± 21.23	83 ± 7
									3	pIRIR_(100, 275)	4.7 ± 0.3	518.3 ± 7.2	110 ± 6
L3478	4	200	3.2	16.5	1.6	23.0	0.16	Quartz	9	OSL-SAR	3.6 ± 0.2	466.2 ± 18.3	129 ± 9
									3(6)	OSL-SMAR		380.4 ± 9.1	105 ± 7
									6(6)	TT-OSL SAR		400.1 ± 24.4	111 ± 9
									4	pIRIR_(100, 275)	4.2 ± 0.2	732.4 ± 60.8	174 ± 17
L3479	4	250	3.8	17.5	1.5	23.0	0.15	Quartz	9	OSL-SAR	3.8 ± 0.2	423.9 ± 7.6	113 ± 7
									3(6)	OSL-SMAR		398.1 ± 8.7	106 ± 7
									6(6)	TT-OSL SAR		396.8 ± 5.3	105 ± 7
									3	pIRIR_(100, 275)	4.4 ± 0.3	458.0 ± 18.8	103 ± 7
L3480	4	300	4.0	19.3	1.4	23.0	0.14	Quartz	9	OSL-SAR	3.9 ± 0.3	442.3 ± 20.1	114 ± 9
									3(6)	OSL-SMAR		423.9 ± 21.9	110 ± 9
									6(6)	TT-OSL SAR		442.2 ± 20.1	114 ± 9
									3	pIRIR_(100, 275)	4.6 ± 0.3	465.2 ± 9.9	101 ± 6
L3481	5	350	3.6	16.7	1.3	23.0	0.13	Quartz	9	OSL-SAR	3.5 ± 0.2	459.6 ± 6.2	133 ± 9
									3(6)	OSL-SMAR		426.9 ± 17.4	123 ± 9
									6(6)	TT-OSL SAR		440.0 ± 9.5	127 ± 9
									5	pIRIR_(100, 275)	4.1 ± 0.2	586.6 ± 74.3	143 ± 20

^aCosmic dose rates (Gy/ka) were calculated according to Prescott and Hutton (1994).

^bNumbers in brackets are the total numbers of aliquots measured.

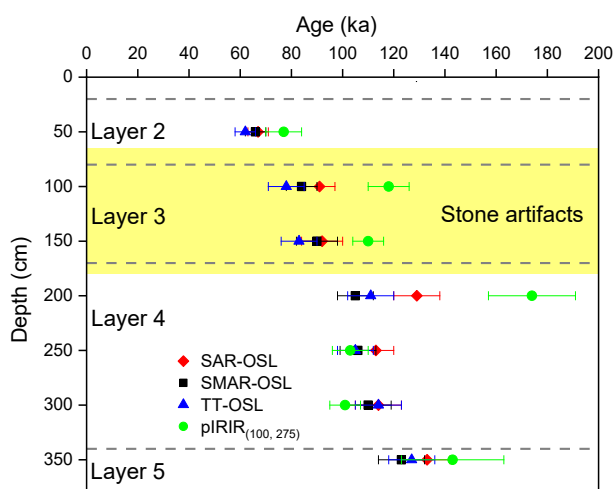


Fig. 6. Age – depth model showing the quartz SAR-, SMAR-, TT-OSL ages and the polymineral pIRIR_(100, 275) ages of the seven samples. The shaded area shows the sedimentary layer where stone artifacts were unearthed.

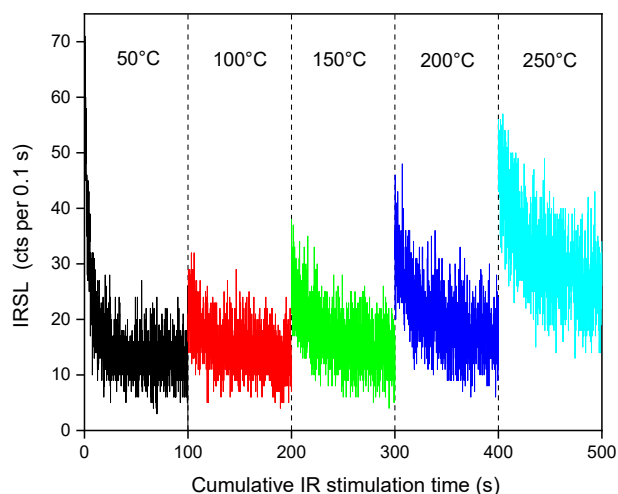


Fig. 7. Decay curves of IRSL (50°C) and MET-pIRIR signals measured at different stimulation temperatures for a single polymineral aliquot of sample L3478.

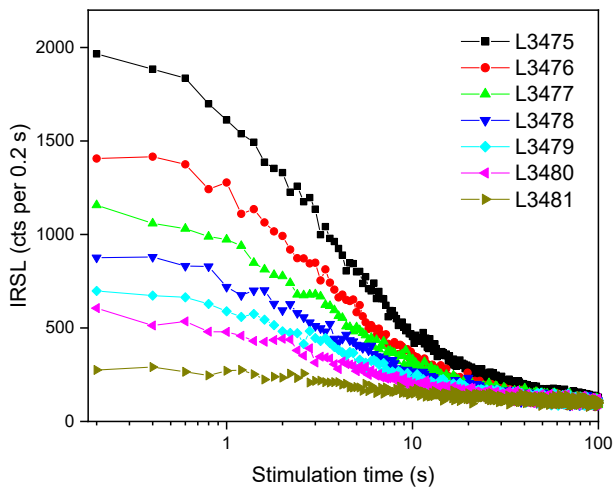


Fig. 8. Natural decay curves of the polymineral $pIRIR_{(100, 275)}$ signals for the study samples.

$pIRIR_{(100, 275)}$ DRCs for the top sample (L3475) and the bottom sample (L3481) shown in **Fig. 9** demonstrate that the two samples are very far from being naturally saturated as the D_0 for samples L3475 and 3481 are 348 Gy and 402 Gy, respectively, and the recycling ratios are scattered but still close to unity. The $pIRIR_{(100, 275)}$ D_e values and ages obtained are summarized in **Table 3** and the ages also shown in **Fig. 6**. The $pIRIR_{(100, 275)}$ ages obtained range from 77 ± 7 to 174 ± 17 ka, and they are not in strict stratigraphical order. The $pIRIR_{(100, 275)}$ ages of samples L3475, L3479, L3480 and L3481 are in agreement with their quartz OSL (SAR-, SMAR- and TT-OSL) ages, if considering 2σ uncertainties. However, the $pIRIR_{(100, 275)}$ ages of samples L3476, L3477 and L3478 are much larger than their corresponding quartz OSL ages. It is noted that the analysis of residual $pIRIR_{(100, 275)}$ dose and fading corrections have not been performed for these samples.

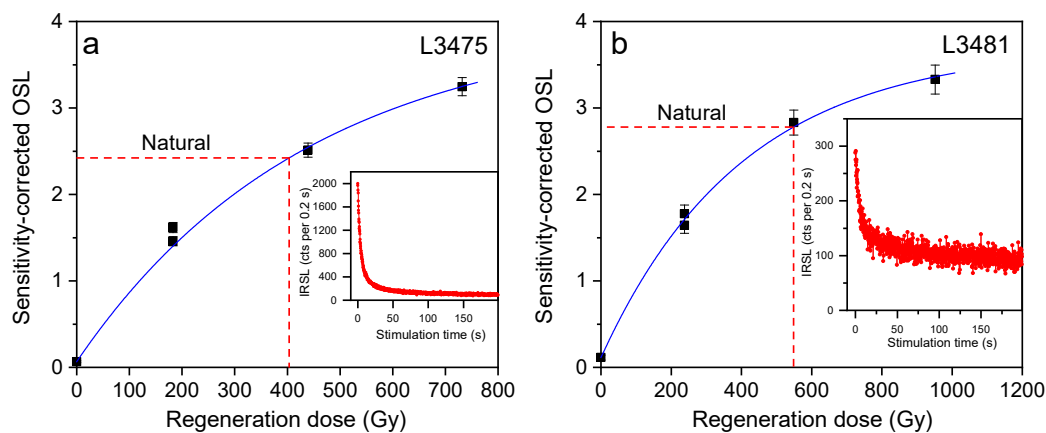


Fig. 9. Dose-response curves of $pIRIR_{(100, 275)}$ signals for single polymineral aliquots of the top sample (L3475, a) and the bottom sample (L3481, b). Insets show the natural decay curves for the two samples.

5. DISCUSSION

The fine quartz extracts from the studied samples demonstrate excellent SAR or SMAR properties such as very bright, fast-dominated component, recycling ratios close to unity, recuperation less than 5% of the corrected natural signal and high saturation dose. The SAR-OSL and SMAR-OSL ages are in stratigraphical order except for the SAR-OSL age of sample L3478 at the depth of 200 cm. Note that although the quartz SAR-OSL D_e values of all samples are slightly larger than their SMAR-OSL D_e values, especially for sample L3478, the SAR- and SMAR-OSL D_e values are consistent when 2σ errors are considered. The slight difference between the SAR- and SMAR-OSL D_e values can be explained by the shapes of their DRCs in **Fig. 2**. This may imply that the quartz SAR-OSL D_e values of our samples were not underestimated due to the build-up of OSL signal during repeated SAR measurement cycles (Zhou and Shackleton, 2001; Lu *et al.*, 2007). However, the large quartz SAR-OSL and SMAR-OSL D_e values ranging from 283 to 466 Gy (**Table 3**, **Fig. 2**) in the high dose range of quartz OSL may be problematic, resulting in underestimation of the true burial age (e.g. Lowick *et al.*, 2015; Timar-Gabor *et al.*, 2017), although some samples yielded reliable quartz SAR-OSL ages with the D_e values of up to 600 Gy, (e.g. Murray *et al.*, 2008; Zhang *et al.*, 2015; Buechi *et al.*, 2017). Here, the reliability of the quartz SAR- and SMAR-OSL ages obtained were tested using the TT-OSL SAR procedure on quartz and the two-step $pIRIR$ and MET- $pIRIR$ procedures on fine polymineral grains, which can potentially extend the age range because TT-OSL and $pIRIR$ signals have very high saturation levels (see reviews by Duller and Wintle, 2012; Li *et al.*, 2014; Arnold *et al.*, 2015).

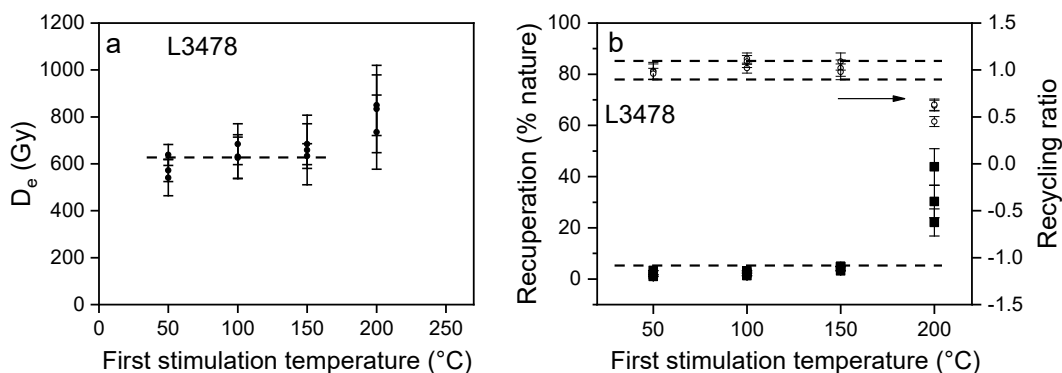


Fig. 10. Plots of $pIRIR_{275} D_e$ values against different sample temperatures for the first IRSL measurements for sample L3478. Three fine polymineral aliquots were measured at each temperature for the IRSL measurements.

TT-OSL signals were considered to be optically bleached at a much slower rate than the fast component OSL signal (Duller and Wintle, 2012), as demonstrated by the results of bleaching experiments on quartz grains with different origins and the TT-OSL D_e values of modern analogues (Tsukamoto *et al.*, 2008; Kim *et al.*, 2009; Athanassas and Zacharias, 2010; Hu *et al.*, 2010; Jacobs *et al.*, 2011; Hernandez *et al.*, 2012; Arnold *et al.*, 2019). The bleaching experiment on a sample in this study shows that the TT-OSL signal was reduced to 50% (equivalent to the D_e value of 230.5 Gy) of its initial value after 1 min bleaching, and 7% (33.4 Gy) after two days of bleaching. Compared with the results of the previous bleaching experiments mentioned above, we considered that the TT-OSL signals from our samples are relatively easily bleached. This is also supported by the fact that the TT-OSL, SAR-OSL and SMAR-OSL D_e values or ages for each sample are almost identical (Table 3, Fig. 6).

Although residual $pIRIR_{(100, 275)}$ doses have not been determined and fading corrections have not been done, their influence on $pIRIR_{(100, 275)} D_e$ values for these old samples are negligible (Li *et al.*, 2014). The stratigraphic inconsistency of the $pIRIR_{(100, 275)}$ ages and the relationship between polymineral $pIRIR_{(100, 275)}$ and quartz OSL ages imply that the $pIRIR_{(100, 275)}$ ages may generally be problematic, this is especially the case for samples L3479 at 250 cm depth and L3480 at 300 cm depth, whose $pIRIR_{(100, 275)}$ ages are younger than the overlying samples (L3476, L3477 and L3478). This may be due to the lower samples are too old (>400 Gy), resulting in underestimation of the $pIRIR$ age (Li and Li, 2012b). Relatively, sample L3476, L3477 and L3478 yielded much larger $pIRIR_{(100, 275)}$ ages compared to the corresponding quartz OSL ages. This is similar to the situation for the samples from the nearby Fengshuzui site (Zhang *et al.*, 2018), where the dim feldspar signal due to the chemical weathering of the sediments was shown to yield 35–55% older ages than those based on the quartz SAR protocol (Huang *et al.*, 2019). In this case, we deduce that the true burial

ages of the upper samples (L3475–3478) are between the quartz OSL ages and the feldspar $pIRIR_{(100, 275)}$ ages.

As stated above, the stone artefacts were mainly excavated mainly from deposits between the lower part of Layer 2 and the upper part of Layer 4 (Figs. 1b and 6), from which samples L3476 and L3477 were collected and optically dated. Their SAR-, SMAR- and TT-OSL ages are indistinguishable when errors are considered, and their average value is 86 ± 9 ka, while the average of the two $pIRIR_{(100, 275)}$ ages is 114 ± 10 ka. These dates bracket the age of the cultural layers. This indicates that this region was occupied by hominins during the marine isotope stage 5.

6. CONCLUSIONS

The Huxushan Paleolithic site in south China was optically dated using various methods, including OSL-SAR, OSL-SMAR and TT-OSL SAR procedures on fine quartz grains and two-step $pIRIR_{(100, 275)}$ and MET- $pIRIR$ procedures on fine polymineral fractions of seven samples from the site. The fine-grained quartz demonstrated excellent luminescence properties, and the SAR-OSL, SMAR-OSL and TT-OSL ages of the studied samples agree with each other and are in stratigraphical order except for one sample. This good internal consistency would indicate that the quartz OSL ages obtained for the samples are reliable. However, the fine polymineral fractions which exhibited dim $pIRIR$ and MET- $pIRIR$ signals yielded older ages for the layer with stone tools. The MET- $pIRIR$ signals are too weak to yield D_e values with useful precision. Although the $pIRIR_{(100, 275)}$ ages obtained for the studied samples are stratigraphically inconsistent, the older ages for the two samples from the cultural layer compared to those derived from quartz SAR OSL protocol are considered to represent the upper age limit of the stone tools. The quartz OSL ages obtained using different procedures for the two samples range from 78 to 92 ka, they are considered as the minimum

age of the cultural layer. The site was deduced to be occupied by hominins during the marine isotope stage 5.

ACKNOWLEDGMENTS

The work was supported by the National Natural Science Foundation of China (Grant No: 41771004) and the National Social Science Fund of China (Grant No: 16CKG005). We are grateful to the anonymous reviewer whose valuable comments and constructive suggestions significantly improved the quality of the manuscript.

REFERENCES

- Aitken MJ and Smith BW, 1988. Optical dating: Recuperation after bleaching. *Quaternary Science Reviews* 7: 387–393, DOI 10.1016/0277-3791(88)90034-0.
- Arnold L, Demuro M, Parés JM, González AP, Arsuaga JL, Castro JMB and Carbonell E, 2015. Evaluating the suitability of extended-range luminescence dating techniques over early and Middle Pleistocene timescales: Published datasets and case studies from Atapuerca, Spain. *Quaternary International* 389: 167–190, DOI 10.1016/j.quaint.2014.08.010.
- Arnold LJ, Demuro M, Spooner NA, Prideaux GJ, McDowell MC, Camens AB, Reedd EH, Parés JM, Arsuaga JL, José María Bermúdez de Castro and Carbonell E, 2019. Single-grain TT-OSL bleaching characteristics: Insights from modern analogues and OSL dating comparisons. *Quaternary Geochronology* 49: 45–51, DOI 10.1016/j.quageo.2018.01.004.
- Athanassas C and Zacharias N, 2010. Recuperated-OSL dating of quartz from Aegean (South Greece) raised Pleistocene marine sediments: current results. *Quaternary Geochronology* 5: 65–75, DOI 10.1016/j.quageo.2009.09.010.
- Bøtter-Jensen L, Andersen CE, Duller GAT and Murray AS, 2003. Developments in radiation, stimulation and observation facilities in luminescence measurements. *Radiation Measurements* 37(4–5): 535–541, DOI 10.1016/S1350-4487(03)00020-9.
- Buechi MW, Lowick SE and Anselmetti FS, 2017. Luminescence dating of glaciolacustrine silt in overdeepened basin fills beyond the last interglacial. *Quaternary Geochronology* 37: 55–67, DOI 10.1016/j.quageo.2016.09.009.
- Buylaert JP, Jain M, Murray AS, Thomsen KJ, Thiel C and Sohbat R, 2012. A robust feldspar luminescence dating method for Middle and Late Pleistocene sediments. *Boreas* 41(3): 435–451, DOI 10.1111/j.1502-3885.2012.00248.x.
- Chu JY, Huang W, Kuang SQ, Wang JM, Xu JJ, Chu ZT, Yang ZQ, Lin KQ, Li P, Wu M, Geng ZC, Tan CC, Du RF and Jin L, 1998. Genetic relationship of populations in China. *Proceedings of the National Academy of Sciences of the United States of America* 95(20): 11763–11768, DOI 10.1073/pnas.95.20.11763.
- Duller GAT and Wintle AG, 2012. A review of the thermally transferred optically stimulated luminescence signal from quartz for dating sediments. *Quaternary Geochronology* 7(1): 6–20, DOI 10.1016/j.quageo.2011.09.003.
- Durcan JA, King GE and Duller GAT, 2015. DRAC: Dose Rate and Age Calculator for trapped charge dating. *Quaternary Geochronology* 28: 54–61, DOI 10.1016/j.quageo.2015.03.012.
- Gao X, 2013. Paleolithic cultures in China: Uniqueness and divergence. *Current Anthropology* 54: 358–370, DOI 10.1086/673502.
- Hernandez M, Mauz B, Mercier N and Shen ZX, 2012. Evaluating the efficiency of TT-OSL SAR protocols. *Radiation Measurements* 47: 669–673, DOI 10.1016/j.radmeas.2012.04.017.
- Hu G, Zhang JF, Qiu WL, and Zhou LP, 2010. Residual OSL signals in modern fluvial sediments from the Yellow River (HuangHe) and the implications for dating young sediments. *Quaternary Geochronology* 5(2–3): 187–193, DOI 10.1016/j.quageo.2009.05.003.
- Hu Y, Marwick B, Zhang JF, Rui X, Hou YM, Yue JP, Chen WR, Huang WW and Li B, 2019. Late Middle Pleistocene Levallois stone-tool technology in southwest China. *Nature* 565: 82–85, DOI 10.1038/s41586-018-0710-1.
- Huang XK, Luo BN and Zhou LP, 2019. Luminescence signals from polymineral fine-grains in strongly chemically-weathered sediments from a Paleolithic site and their usefulness for dating[J]. *Quaternary Sciences* 39, DOI 10.11928/j.issn.1001-7410.2019.02.16.
- Huntley DJ, Godfrey-Smith DI and Thewalt MLW, 1985. Optical dating of sediments. *Nature* 313: 105–107, DOI 10.1038/313105a0.
- Jacobs J, Roberts RG, Lachlan TJ, KarkanasPb, Marean CW and Roberts DL, 2011. Development of the SAR TT-OSL procedure for dating Middle Pleistocene dune and shallow marine deposits along the southern Cape coast of South Africa. *Quaternary Geochronology* 6: 491–513, DOI 10.1016/j.quageo.2011.04.003.
- Kim JC, Duller GAT, Roberts HM, Wintle AG, Lee YI and Yi SB, 2009. Dose dependence of thermally transferred optically stimulated luminescence signals in quartz. *Radiation Measurements* 44: 132–143, DOI 10.1016/j.radmeas.2008.12.001.
- Lai ZP and Brückner H, 2008. Effects of feldspar contamination on equivalent dose and the shape of growth curve for OSL of silt-sized quartz extracted from Chinese loess. *Geochronometria* 30(1): 49–53, DOI 10.2478/v10003-008-0010-0.
- Li B and Li SH, 2011. Luminescence dating of K-feldspar from sediments: A protocol without anomalous fading correction. *Quaternary Geochronology* 6(5): 468–479, DOI 10.1016/j.quageo.2011.05.001.
- Li B and Li SH, 2012a. Luminescence dating of Chinese loess beyond 130 ka using the non-fading signal from K-feldspar. *Quaternary Geochronology* 10: 24–31, DOI 10.1016/j.quageo.2011.12.005.
- Li B and Li SH, 2012b. A reply to the comments by Thomsen et al. on “Luminescence dating of K-feldspar from sediments: A protocol without anomalous fading correction”. *Quaternary Geochronology* 8: 49–51, DOI 10.1016/j.quageo.2011.10.001.
- Li B, Jacobs, Z, Roberts, RG and Li, SH, 2014. Review and assessment of the potential of post-IR IRSL dating methods to circumvent the problem of anomalous fading in feldspar luminescence. *Geochronometria* 41(3): 178–201, DOI 10.2478/s13386-013-0160-3.
- Li ZY, Wu XJ, Zhou LP, Liu W, Gao X, Nian XM and Trinkaus E, 2017. Late Pleistocene archaic human crania from Xuchang, China. *Science* 355: 969–972, DOI 10.1126/science.aal2482.
- Liu C, Xu XM, Yuan BY and Deng CL, 2008. Magnetostratigraphy of the Qiliting section (SE China) and its implication for geochronology of the red soil sequences in southern China. *Geophysical Journal International* 174: 107–117, DOI 10.1111/j.1365-246X.2008.03814.x.
- Liu W, Martínón-Torres M, Cai YJ, Xiong S, Tong XH, Pei SW, Sier MJ, Wu XH, Edwards LE, Cheng H, Li YY, Yang XX, Bermúdez de Castro JM and Wu XJ, 2015. The earliest unequivocally modern humans in southern China. *Nature* 526: 696–699, DOI 10.1038/nature15696.
- Lowick SE, Buechi MW, Gaar D, Graf HR and Oreusser F, 2015. Luminescence dating of Middle Pleistocene proglacial deposits from northern Switzerland: methodological aspects and stratigraphical conclusions. *Boreas* 44(3): 459–482, DOI 10.1111/bor.12114.
- Lu HY, Zhang HY, Wang SJ, Cosgrove R, Sun XF, Zhao J, Sun DH, Zhao C, Shen C and Wei M, 2011. Multiphase timing of hominin occupations and the paleoenvironment in Luonan Basin, Central China. *Quaternary Research* 76: 142–147, DOI 10.1016/j.yqres.2011.04.001.
- Lu YC, Wang XL and Wintle AG, 2007. A new OSL chronology for dust accumulation in the last 130,000 yr for the Chinese Loess Plateau. *Quaternary Research* 67(1): 152–160, DOI 10.1016/j.yqres.2006.08.003.
- Murray AS, Buylaert JP, Henriksen M, Svendsen JI and Mangerud J, 2008. Testing the reliability of quartz OSL ages beyond the Eemian. *Radiation Measurements* 43(2–6): 776–780, DOI 10.1016/j.radmeas.2008.01.014.
- Murray AS and Wintle AG, 2000. Luminescence dating of quartz using an improved single-aliquot regenerative-dose protocol. *Radiation Measurements* 32(1): 57–73, DOI 10.1016/S1350-4487(99)00253-X.

- Murray AS and Wintle AG, 2003. The single aliquot regenerative dose protocol: Potential for improvements in reliability. *Radiation Measurements* 37(4–5): 377–381, DOI 10.1016/S1350-4487(03)00053-2.
- Piazza, 1998. Towards a genetic history of China. *Nature* 395: 636–639, DOI 10.1038/27071.
- Prescott JR and Hutton JT, 1994. Cosmic ray contributions to dose rates for luminescence and ESR dating: Large depths and long-term time variations. *Radiation Measurements* 23(2–3): 497–500, DOI 10.1016/1350-4487(94)90086-8.
- Roberts RG, Jacobs Z, Li B, Jankowski NR, Cunningham AC and Rosenfeld AB, 2015. Optical dating in archaeology: thirty years in retrospect and grand challenges for the future. *Journal of Archaeological Science* 56: 41–60, DOI 10.1016/j.jas.2015.02.028.
- Slimak L, Svendsen JI, Mangerud J, Plisson H, Heggen HP, Brugère A and Pavlov PY, 2011. Late Mousterian Persistence near the Arctic Circle. *Science* 332: 841–845, DOI 10.1126/science.1203866.
- Sun XF, Lu HY, Wang SJ and Yi SW, 2012. Ages of Liangshan Paleolithic sites in Hanzhong Basin, central China. *Quaternary Geochronology* 10: 380–386, DOI 10.1016/j.quageo.2012.04.014.
- Thiel C, Buylaert JP, Murray AS, Terhorst B, Hofer I, Tsukamoto S and Frechen M, 2011. Luminescence dating of the Stratzing loess profile (Austria) – Testing the potential of an elevated temperature post-IR IRSL protocol. *Quaternary International* 234(1–2): 23–31, DOI 10.1016/j.quaint.2010.05.018.
- Thomsen KJ, Murray AS, Jain M and Bøtter-Jensen L, 2008. Laboratory fading rates of various luminescence signals from feldspar-rich sediment extracts. *Radiation Measurements* 43(9–10): 1474–1486, DOI 10.1016/j.radmeas.2008.06.002.
- Timar-Gabor A, Buylaert JP, Guralnik B, Trandafir–Antohei O, Constantin D, Anechitei-Deacu V, Jain M, Murray AS, Porat N, Hao Q and Wintle AG, 2017. On the importance of grain size in luminescence dating using quartz. *Radiation Measurements* 106: 464–471, DOI 10.1016/j.radmeas.2017.01.009.
- Tsukamoto S, Geoff AT, Duller GAT and Wintle AG, 2008. Characteristics of thermally transferred optically stimulated luminescence (TT-OSL) in quartz and its potential for dating sediments. *Radiation Measurements* 43: 1204–1218, DOI 10.1016/j.radmeas.2008.02.018.
- Wang CC and Li H, 2013. Inferring human history in East Asia from Y chromosomes. *Investigative Genetics* 4: 11, DOI 10.1186/2041-2223-4-11.
- Wang XL, Lu YC and Wintle AG, 2006. Recuperated OSL dating of fine-grained quartz in Chinese loess. *Quaternary Geochronology* 1(2): 89–100, DOI 10.1016/j.quageo.2006.05.020.
- Zhang JF, Huang WW, Hu Y, Yang SX and Zhou LP, 2015. Optical dating of flowstone and silty carbonate-rich sediments from Panxian Dadong Cave, Guizhou, southwestern China. *Quaternary Geochronology* 30: 479–486, DOI 10.1016/j.quageo.2015.01.011.
- Zhang JF, Li YY, Han YS, Wang JK and Zhou LP, 2018. Luminescence dating of weathered sediments from the Paleolithic site of Fengshuzui in northern Hunan province, China. *Quaternary Geochronology* 49: 211–217, DOI 10.1016/j.quageo.2018.07.003.
- Zhang JF and Zhou LP, 2007. Optimization of the 'double SAR' procedure for polymineral fine grains. *Radiation Measurements* 42(9): 1475–1482, DOI 10.1016/j.radmeas.2007.06.007.
- Zhou LP and Shackleton, 2001. Photon-stimulated luminescence of quartz from loess and effects of sensitivity change on palaeodose determination. *Quaternary Science Reviews* 20(5–9): 853–857, DOI 10.1016/S0277-3791(00)00024-X.
- Zhu RX, Potts R, Pan YX, Yao HT, Lü LQ, Zhao X, Gao X, Chen LW, Gao F and Deng CL, 2008. Early evidence of the genus Homo in East Asia. *Journal of Human Evolution* 55: 1075–1085, DOI 10.1016/j.jhevol.2008.08.005.